The Benzyl Radical–Ethylene Molecular Cluster: An Example of Electronic-State Mediation of Chemical Reactivity

R. Disselkamp[†] and E. R. Bernstein[*]

Department of Chemistry, Colorado State University, Fort Collins, Colorado 80523

Received: November 29, 1993[⊕]

Three types of experimental data are presented for the benzyl radical/ethylene molecular cluster: mass-resolved excitation spectra (MRES), ionization energy threshold determination, and excited-state lifetime measurements at different excitation energies. MRES of benzyl radical $(C_2H_4)_{1,2}$ exhibit broad features in the $D_1 \leftarrow D_0$ benzyl radical absorption region that extend beyond 11 810 cm^{-1} of vibrational energy in D_1. The ionization threshold for the one-to-one cluster is shifted by -1160 cm^{-1} relative to that of the bare benzyl radical. Cluster excited-state lifetime measurements indicate a shortened lifetime at higher excitation energy. This collection of benzyl radical/ethylene data differs greatly from that of the previously studied benzyl radical/ethane cluster system. These latter results consist of well-resolved spectroscopic structure with low-energy van der Waals modes and molecular vibrations, a small shift in ionization energy relative to the bare benzyl radical of ~-50 cm^{-1}, and vibrational predissociation at roughly 700 cm^{-1} of vibrational energy in D_1. The anomalous benzyl radical/ethylene data can be explained if one postulates that an excited-state bimolecular addition chemical reaction occurs between benzyl radical and ethylene upon optical excitation of the benzyl radical $(D_2, D_1 \leftarrow D_0)$. *Ab initio* calculational results are presented which support the assertion of an apparent excited-state chemical reaction. Finally, unimolecular dissociation rate theories are used to extract an excited-state "binding energy" for the benzyl radical/ethylene "cluster" from excited-state lifetimes.

I. Introduction

The study of cluster photochemistry addresses the effect of both reactant energy and orientation on chemical reactivity.[1-3] Electronic excitation can be used to enhanced or alter chemical reactivity in two different ways. First, the reactants can remain on an excited potential energy surface whose energy barrier to reaction is less than the internal energy of the reactants. Second, following electronic excitation, the reactants can internally convert to the ground state and in so doing acquire enough internal energy to surmount the ground electronic state barrier to reaction. The majority of the literature pertaining to bimolecular excited electronic state reactivity deals with electron-transfer, proton-transfer, hydrogen atom abstraction, or photosubstitution reactions.

In addition to characterization of the energy dependence of a reaction, the spatial orientation of reactants or the "reaction coordinate" can be examined. For bimolecular reactions studied in crossed molecular beams, the use of external electromagnetic fields has been employed to control initial reactant orientations.[4-10] Reactant orientation can also be controlled by generation of a van der Waals complex of the two reactant species; the subsequent absorption of a photon by one of the two molecules in the cluster can initiate the chemical reaction. A classic study along these latter lines is the photodissociation of hydrogen bromide contained in the $CO_2\cdots(HBr)_1$ complex.[11] The products of this photochemically initiated reaction are CO and OH. Laser-induced fluorescence (LIF) techniques are employed to probe the OH product-state distribution. The observed differences between cluster and bulk gas-phase results can be attributed to the restricted orientations found in the van der Waals complex.

A variety of *ab initio* computational studies of bimolecular addition reactions have been performed over the past decade.[12-18] Some of these investigations identify a particular reaction path to be favorable among many possibilities, yielding valuable insight for experimental studies unable to discriminate between different reaction pathways.[12,13] The preferred calculational approach

taken to account for the salient features of chemical bonding is the multiconfiguration self-consistent-field (MCSCF) technique: adiabatic reaction potential surfaces are thereby explored. Dynamic electron correlation effects must be included in the algorithm using either perturbational (i.e., inclusion of Moller-Plesset wave function corrections) or multireference configuration interaction (MRCI) approaches in order to obtain quantitatively accurate bond energies. A reliable double-ζ basis set is appropriate for these calculations to minimize basis set superposition errors (BSSE). Fulfilling these requirements is computationally expensive, and so information of a more qualitative nature is often the compromise.

In this report we present an experimental and *ab initio* theoretical study of chemical reactivity for the benzyl radical/ethylene cluster system. In particular, the effect of electronic excitation of long-lived valence states ($\tau > 1$ μs) on chemical reactivity is explored. We argue that supersonic jet cooling of a photolyzed precursor (benzyl radical) in an ethylene-seeded helium expansion gas generates a cold van der Waals cluster (benzyl radical (ethylene)$_1$) which undergoes a radical addition reaction upon optical excitation. Since the proposed reaction is an excited-state bimolecular addition reaction generating a comparatively large product complex, a straightforward product-state distribution analysis cannot be readily performed. In fact, the distance the reactants travel along the reaction coordinate (that is, the extent of reaction) cannot be directly determined. The reaction exothermicity is presumably to be transformed into internal (thermal) energy of the product complex. Three pieces of experimental evidence are found for this cluster system which support the occurrence of an excited-state photochemical addition reaction: (1) Frank–Condon broadened excitation spectrum for the cluster, (2) reduced (by more 10^3 cm^{-1}) ionization energy compared to that observed for both the unclustered benzyl radical and the benzyl radical/ethane cluster, and (3) a roughly 7000-cm^{-1} apparent "binding energy" for the excited-state benzyl radical/ethylene cluster.

In this effort, both the methyl radical/ethylene and benzyl radical/ethylene reacting systems are explored by *ab initio* computational techniques. The smaller system (methyl radical

---

plus ethylene) is examined as an internal calibration for these calculations since it is amenable to high-level computation. We explore this system at the complete active space self-consistent-field (CASSCF) MRCI (singles and doubles) level to obtain a calibration of the quantitative accuracy of our calculational approach, before proceeding with CASSCF benzyl radical/ethylene calculations. The effect of dynamic electron correlation for the benzyl radical/ethylene system is approximated for the ground electronic state by performing spin-projected[19] MP2 calculations for both the methyl radical/ethylene (calibration) and benzyl radical/ethylene system. In essence, we approximate a correction to the benzyl radical/ethylene excited-state CASSCF results with the ground-state dynamic electron correlation energy; based on the MRCI methyl radical/ethylene results, this procedure is expected to underestimate the importance of dynamic electronic correlation for the excited state.

The addition of methyl radical to ethylene has been examined previously using restricted-Hartree–Fock (RHF) and unrestricted-Hartree–Fock (UHF) techniques.[20] Subsequent higher-level calculations have been performed using spin-projected UHF (PUHF) and perturbational (PMP2, PMP3, PMP4) techniques.[21] By accounting for dynamic electron correlation using Moller–Plesset perturbational techniques, one obtains good agreement with the experimentally measured barrier height and reaction enthalpy. A comparison between these previous calculational approaches and the one used in our work will be given. In the present work both ground- and excited-state adiabatic potential energy surfaces are of concern and are explored.

We begin this report with a discussion of the experimental and computational procedures used. Following this, we present and interpret the experimental results, introduce a model for the excited-state reaction between oriented benzyl radical and ethylene, discuss *ab initio* calculational support for the model, and finally present RRKM dissociation rate constant calculations to achieve an estimate of the excited-state "cluster binding energy" or "incipient bond" formation between benzyl radical and ethylene.

II. Procedures

A. Experiments. In a previous report we outlined the generation and spectroscopic study of the benzyl radical and its clusters with Ar, N_2, CH_4, C_2H_6, and C_3H_8.[1] Since the experimental techniques used in that study are only slightly different from those used here, a brief overview of these techniques, with an emphasis on the differences between the previous studies and those of this effort, is presented below.

Three different types of experiments are carried out for the benzyl radical/ethylene system as presented schematically in Figure 1: (1) mass-resolved excitation spectra (MRES), which in essence yields mass-resolved electronic absorption information obtained by scanning λ_1 and fixing λ_2; (2) ionization potential threshold spectra acquired by fixing λ_1 to an optical transition and scanning λ_2; and (3) time-delayed excitation/ionization laser studies, which measure excited electronic-state lifetimes by tuning the wavelength of the excitation laser (λ_1) to an optical resonance and measuring the ion signal for the appropriate mass as a function of time delay between the excitation and ionization (λ_1 and λ_2) lasers. For these studies the ionization laser counterpropagates on the molecular beam axis via a turning prism located inside the vacuum chamber, which has been shown to measure lifetimes accurately up to ~ 3 μs.[22]

Signal is acquired as follows. Radiation from a Questek Series 2000 excimer laser equipped with ArF gas (193 nm) is focused with a 50-cm-focal length lens onto the exit region of an R.M. Jordan pulsed valve operating at 10 Hz. Helium is used as the expansion gas with nozzle backing pressures ranging from 20 to 80 psig. Cluster species are generated by using an expansion mixture containing either 1% or 10% of the clustering agent
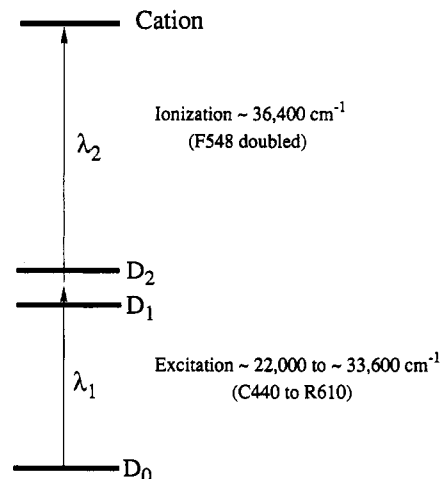

Figure 1. Schematic illustration of experimental techniques used in this work: 1, mass-resolved excitation spectroscopy (MRES) (scan λ_1, fix λ_2); 2, ionization potential determination (fix λ_1, scan λ_2); 3, laser delay probe of excited-state lifetime (scan Δt between λ_1 and λ_2).

(solvent molecule) of interest in helium. The photolyzed precursors generated in the high-density region of the expansion cool, cluster as appropriate, pass through a skimmer, and travel between a pair of ion extraction plates for the time-of-flight mass spectrometer. This cold molecular beam intersects two spatially and temporally overlapped lasers. The first laser excites the D_2, $D_1 \leftarrow D_0$ transition of the radicals, and the second laser ionizes the electronically excited species. The generated ions are extracted at 250 V and accelerated by ~ 4 kV into a 1.5-m flight tube and are focused onto a Gallileo Electro-Optics microchannel plate (MCP) detector. Since an ion's flight time is related to the square root of its mass, mass resolution is achieved by selective gated integration. Calibration of the mass spectrometer is performed during the course of the experiments by generating aniline–$(NH_3)_n$ clusters with $n = 0$–5. Within this mass range the ion masses are uniquely determined.

Triggering of the nozzle, lasers, oscilloscope, and data acquisition peripherals is accomplished using two Stanford Research Systems four-channel digital delay generators. The excitation and ionization lasers are Spectra Physics Nd:YAG pumped dye lasers equipped with wavelength extension accessories. A variety of laser dyes, all purchased from Exciton, are used for the excitation laser: these include Exalite 392E and 400E, Coumarin 440 and 460, Stilbene 420, and Rhodamine 610 (frequency doubled). For the ionization laser, Fluorescence 548 and Rhodamine 575 (both frequency doubled) are used. Precursor samples are purchased from Aldrich Chemical Co. and are used without additional purification.

B. Calculations. *Ab initio* results will be presented in the next section using different levels of wave function approximation to explore the electronic-state dependence of chemical reactivity within the methyl radical/ethylene and benzyl radical/ethylene cluster species. Since a unique one-dimensional reaction coordinate is assumed for these species, adiabatic potential energy surfaces can be obtained from reaction and activation energies in a straightforward manner. Calculations are performed using the HONDO,[23] MESA,[24] and GAUSSIAN[25] series of programs running on two IBM RISC/6000 320H workstations equipped with 64 and 80 MB of memory and 3 GB of disk storage space.

Geometry optimization results are obtained by reducing analytically determined energy gradients to less than 0.0005 au. Calculational results presented here are obtained with the Dunning–Huzinaga [9s/5p]/[3s/2p] double-zeta valence (DZV) basis.[26] RHF and restricted open-shell Hartree–Fock (ROHF) results are used to explore ground electronic state reaction energies for benzyl radical/ethylene reactant species and determine BSSE errors via the counterpoise technique.
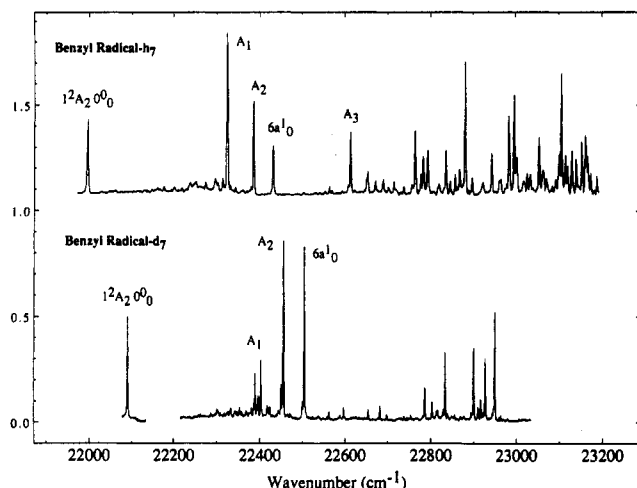
Figure 2. Two-color MRES of benzyl-h_7 and -d_7 radicals formed from the photolysis of benzyl chloride and cooled in the supersonic expansion. The 0_0^0 transitions are at 21 998 (h_7) and 22 090 cm^{-1} (d_7).

Higher level CASSCF calculations for both the methyl radical/ethylene and benzyl radical/ethylene system are also performed. Identifying the π orbitals to include in the CASSCF calculations is straightforward; however, to obtain the σ and σ^* orbitals for the bond being formed, one must perform fixed point calculations with the relevant bond stretched. The resulting highest occupied and lowest unoccupied orbitals correspond to the σ and σ^* orbitals of this extended bond, together with the π orbitals, are used to generate an initial orbital guess. For methyl radical/ethylene, the lowest two electronic states of the system are examined: these states are the ground state and an electronically excited *ethylene* reactant species. Results for the lowest three electronic states of the benzyl radical/ethylene system are presented which correspond to different electronic configurations of the *benzyl radical* reactant. Dynamic electron correlation energies are obtained for the methyl radical/ethylene system from multireference single and double excitations (MESA) using the CASSCF wave function (MRCI/S+D).

By performing PMP2 calculations (Gaussian) on both the methyl radical/ethylene (calibration system) and benzyl radical/ethylene reacting systems, the effect of dynamic electron correlation for ground electronic state benzyl radical/ethylene (obtained from difference of PMP2 and PUHF results) can be obtained and used to approximate excited-state dynamic electron correlation results.

III. Results and Discussion

In this section we present the experimental results for benzyl radical–$(C_2H_4)_{1,2}$ clusters, put forth a model for the observed behavior, and explore this model with *ab initio* calculations.

A. Experiments. *1. MRES of Photolyzed Precursors.* Two-color MRES of benzyl-h_7 radical[27] and benzyl-d_7 radical obtained from benzyl chloride precursors are presented in Figure 2. Experimental data for the benzyl-h_7 radical species is the same as reported earlier.[27] The MRES of benzyl-d_7 radical supersonically cooled has not been reported previously. Both spectra exhibit an electronic origin for the $D_1 \leftarrow D_0$ ($1^2A_2 \leftarrow 1^2B_2$) transition, intense features 300–650 cm^{-1} to the blue of this origin arising in part from 1^2A_2–1^2B_2 vibronic coupling (labeled "A_n"), and mixed vibronic features to higher energy. A vibronic analysis of both spectra has been performed by Cossart-Magos and Leach[28] and more recently by Negri et al.[29] Our spectra generally support these analyses with two exceptions: additional spectroscopic structure for benzyl-d_7 radical accompanying the feature labeled A_1 is not predicted, and the observed low intensity of the benzyl-d_7 radical A_3 feature (not assigned) is not predicted by Negri et al.[29] Although the predicted and observed intensity of the A_1

feature of benzyl-d_7 radical is comparatively weak, increasing the backing gas pressure from 30 to 60 psig results in identical spectra, implying that the presence of additional spectroscopic structure accompanying this feature is unlikely due to hot band absorption.

Of particular interest here regarding these spectra is the formation of cold radical species following photolysis at the nozzle. Additional photolysis product MRES data are collected utilizing various precursor species: results of such experiments are given in Table 1. For the sake of brevity, these spectra are not presented. Independent of the precursor, only well-resolved spectroscopic structure is observed; no hot bands accompany the electronic origins, indicating that complete cooling occurs following photolysis. Table 1 shows that photolysis of propylbenzene leads to the observation of two product species: styrene and *trans-β*-methylstyrene. Spectra of both of these species are obtained with a signal-to-noise ratio equivalent to published spectra of each molecule,[30,31] indicating a high photoconversion efficiency to products and complete cooling. Also listed in Table 1 is the observed product branching ratio determined by signal height comparison for the most intense feature near the electronic origin of each species. The calculated reaction endothermicities presented in Table 1 are obtained from Benson's tables;[32] these endothermicities used in a unique single-exponential function reproduce all the observed product branching ratios of species formed from different precursors. This result implies that the photolysis conditions are reproducible and that a correlation exists between reaction endothermicities and products formed in this manner.

The supersonic expansion has the capacity to cool very "hot" chemical reaction products. If conversion of a precursor species to products is through a one-photon process (it may well involve absorption of many photons), the reactant in the photochemical process absorbs 148.0 kcal/mol ($\lambda \sim 193$ nm) of energy. The most endothermic reaction listed in Table 1 for an observed product is the photolysis of benzyl chloride to α-chlorobenzyl radical and a hydrogen atom. Therefore, a *minimum* of 67.5 kcal/mol of energy minus translational energy of the separating fragments is left in the generated products. The hot product is effectively cooled during the supersonic expansion process.

2. MRES of Benzyl Radical Clusters. Benzyl radical– $(C_2H_6)_1$. Two-color MRES of benzyl radical–$(C_2H_6)_1$ is presented in Figure 3.[1] A detailed discussion of the benzyl radical–$(C_2H_6)_1$ cluster species as well as the benzyl radical clustered with the solvents Ar, N_2, CH_4, and C_3H_8 has been published previously.[1] The spectrum presented in Figure 3 is similar to that found for other benzyl radical clusters with regard to line width, resolution, intensity, and the features observed.[1] The two-color MRES of benzyl radical–$(C_2H_6)_1$ is distinguished from that of the bare benzyl radical (Figure 2) by van der Waals vibrational structure near the cluster origin, perturbed vibronic intensities below 0_0^0 + 500 cm^{-1} (especially, 0_0^0, A_1, A_2), and the absence of absorption intensity to higher energy than 22 600 cm^{-1}. This decrease in signal at high energy can be attributed to vibrational predissociation of the cluster.[1] A small change in ionization energy threshold of benzyl radical–$(C_2H_6)_1$ relative to the bare benzyl radical of –50 cm^{-1}, close to the $D_1 \leftarrow D_0$ spectral shift upon clustering, is also observed. These observations are characteristic of a van der Waals (weakly bound) cluster present in the ground and optically excited electronic state.

Benzyl Radical–$(C_2H_4)_n$. Two-color MRES of benzyl radical–$(C_2H_4)_n$ clusters are presented in Figures 4 and 5. These spectra are quite different than those observed for the bare benzyl radical and benzyl radical–$(C_2H_6)_1$ cluster spectra with regard to line width, extent, and required threshold ionization energy. The similarities between the benzyl radical–$(C_2H_4)_1$ and benzyl radical–$(C_2H_4)_2$ cluster spectra in Figure 4 indicate that the onset of spectral broadening occurs with the formation of the one-to-

TABLE 1: Observed and Calculated Nozzle Photochemistry Products and Branching Ratios

precursor	product	observed product branching ratio (%)	ΔH (kcal/mol)	calculated product[a] (%)
propylbenzene	styrene + methane	~70	14.2	71
	β-methylstyrene + H_2	~30	23.2	29
	α-ethylbenzyl radical + H	0	86.7	0
benzyl chloride	benzyl radical + Cl	~85	65.5	82
	α-chlorobenzyl radical + H	~15	80.5	18
cumene (isopropyl-benzene)	α,α-dimethylbenzyl radical	~5	71.0	1
	α-methylbenzyl radical	~95	19.4	99

[a] Obtained using enthalpies of reaction, ΔH, a temperature of 5040 K, and a Boltzmann distribution function (see text).
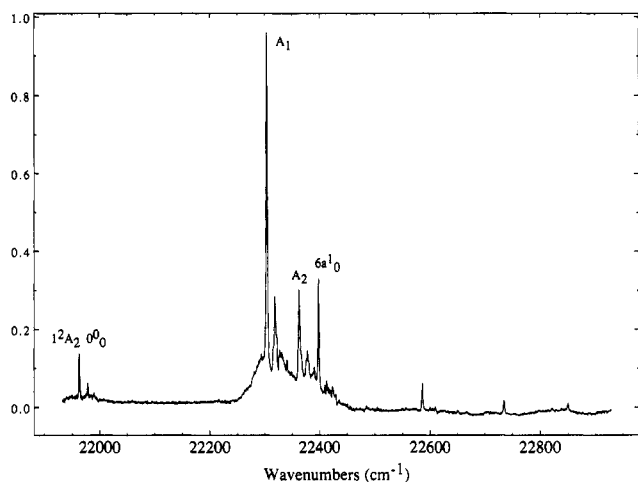

Figure 3. Two-color MRES of benzyl radical–$(C_2H_6)_1$ cluster obtained from photolyzing benzyl chloride and expanding with 1% ethane in helium. Note the loss of intensity beyond 22 600 cm^{-1}.
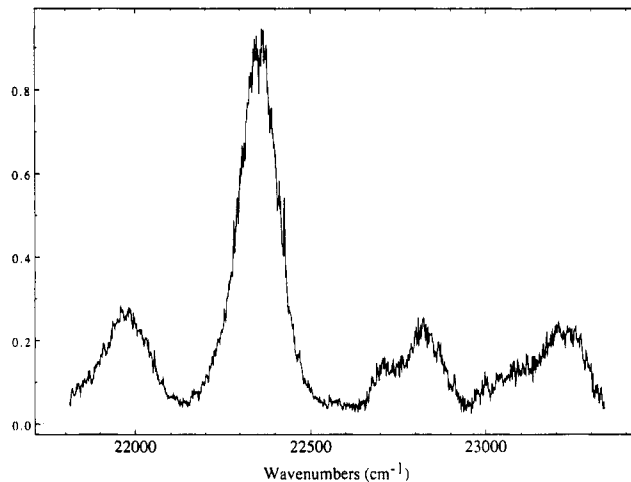

Figure 5. Two-color MRES of benzyl-d_7 radical–$(C_2H_4)_1$, obtained from photolyzing deuterated benzyl chloride and expanding with 1% ethylene in helium.
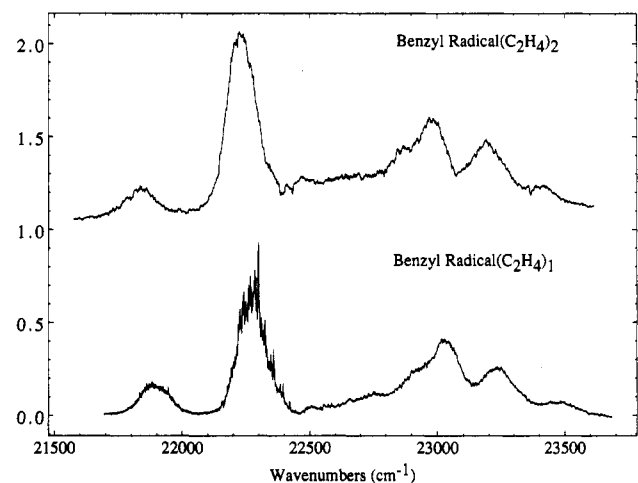

Figure 4. Two-color MRES of benzyl radical–$(C_2H_4)_n$ ($n = 1, 2$) obtained from photolyzing benzyl chloride and expanding with 1% C_2H_4 in helium.

TABLE 2: Relative Signal Levels for Benzyl Radical Cluster Species

expansion mixture//species	feature excited or excitation energy (cm^{-1})	normalized signal (cm^{-1})
10% C_2H_6 in helium		
benzyl radical	A_1	1.0
benzyl radical–$(C_2H_6)_1$	A_1	0.044
benzyl radical–$(C_2H_6)_2$	A_1	<0.011
10% C_2H_4 in helium		
benzyl radical	A_1	1.0
benzyl radical–$(C_2H_4)_1$	22 300	0.60
benzyl radical–$(C_2H_4)_2$	22 200	0.12
benzyl radical–$(C_2H_4)_3$	22 100	0.067
1% C_2H_4 in helium		
benzyl radical	A_1	1.0
benzyl radical–$(C_2H_4)_1$	22 300	0.42
benzyl radical–$(C_2H_4)_1$	32 780	0.083
benzyl radical–$(C_2H_4)_2$	22 200	0.017
benzyl radical–$(C_2H_4)_3$	–	–

one cluster species. The observed carrier of this spectrum is most likely a benzyl radical-like moiety because the benzyl radical/C_2H_4 spectra fall in the same energy region as those of the benzyl radical itself and benzyl radical van der Waals cluster systems. The benzyl-d_7 radical–$(C_2H_4)_1$ spectrum of Figure 5 demonstrates that benzyl radical deuteration has little effect on the observed cluster spectrum.

Additional spectra of the benzyl radical–$(C_2H_4)_1$ cluster show that nontunable, spectrally broad cluster signal is observed even at an excitation energy of 33 610 cm^{-1}, or 11 810 cm^{-1} of vibrational energy in D_1: beyond this energy, cluster signal dramatically decreases. At an excitation energy of 36 200 or 14 400 cm^{-1} excess vibrational energy in D_1, no cluster signal is observed. This result suggests that a large interaction energy between electronically excited benzyl radical and ethylene occurs

in the cluster. The observed enhancement in interaction (i.e., binding) energy not only contrasts with the benzyl radical–$(C_2H_6)_1$ result but also to our knowledge has not been observed to this extent for any cluster species. The loss of cluster signal at ca. 12 000 cm^{-1} above the spectral onset for the cluster can be interpreted and analyzed with regard to a dissociation mechanism such as RRKM theory[33-38] in order to extract a cluster "binding energy" in the excited state. This analysis is presented below.

Table 2 lists normalized signal intensities for the benzyl radical–$(C_2H_6)_1$ and benzyl-h_7 radical–$(C_2H_4)_n$ cluster species obtained from different mixtures of C_2H_6 or C_2H_4 in helium. Two important results can be extracted from the data listed in Table 2. First, a comparison between the cluster signal intensities for the 10% and 1% ethylene/helium mixtures shows fragmentation from benzyl radical–$(C_2H_4)_2$ and higher-order clusters does not affect the data for the benzyl radical–$(C_2H_4)_1$ species. Second,
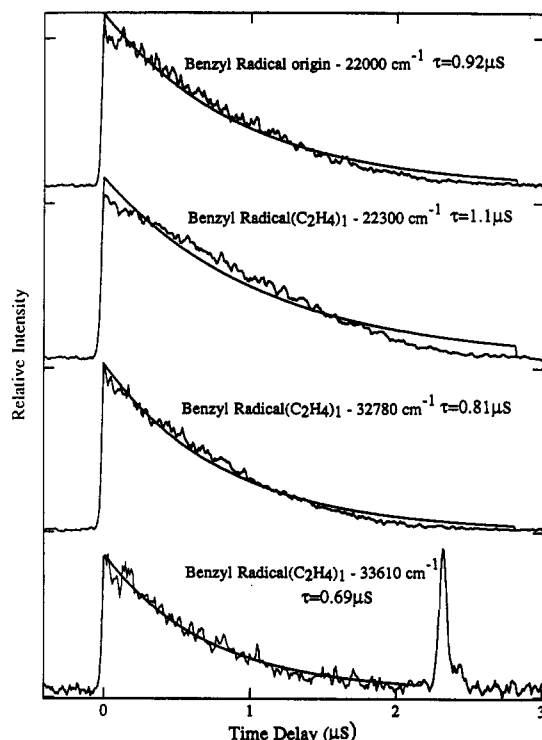
Figure 6. Excited electronic state lifetimes of bare benzyl radical and benzyl radical–$(C_2H_4)_1$ cluster species obtained by scanning laser delay between excitation and ionization lasers and by increasing the pump excitation energy. The intense feature in the bottom decay is due to a one-color signal of aniline that falls into the delayed signal mass channel.

Figure 7. Ionization potential threshold spectra of the benzyl radical–$(C_2H_4)_1$ cluster. The onset of ion signal occurs at 57 200 cm^{-1}.

an anomalously intense benzyl radical–$(C_2H_4)_1$ signal is observed compared to the benzyl radical–$(C_2H_6)_1$ signal is observed compared to the benzyl radical–$(C_2H_6)_1$ signal; the latter signal level is typical for weakly bound van der Waals species. This intensity anomaly is most likely not due to a greater concentration of benzyl radical–$(C_2H_4)_1$ in the expansion following photolysis, since empirical potential energy calculations of van der Waals cluster binding energies for benzyl radical/ethylene[39] and ethane[1] clusters yield cluster binding energies of 736 and 708 cm^{-1}, respectively. Plausible explanations for the anomalously high signal intensity of the benzyl radical/ethylene clusters include an enhancement in either the excitation or ionization optical cross section(s).

Figure 6 presents the results of a two laser delay pump/probe study of the excited state of the bare benzyl radical and of the benzyl radical–$(C_2H_4)_1$ cluster at various excitation energies. The smooth curves in this figure represent a least-squares fit of a single-exponential function to the data by fixing only the zero signal level and optimizing the remaining two parameters (I_{max} and τ). The excited-state lifetimes of both species at the reported excitation energies near the origin transition are similar and likely reflect differences due to experimental errors and fitting. The top two decay curves presented in Figure 6 are not well fit to single-exponential decays as has been pointed out previously.[27,40] The bare benzyl radical lifetime has been studied in a supersonic expansion using laser-induced fluorescence[27,40] and MRES.[27] The observed dual-exponential behavior ($\tau_{short} \sim 0.4$ μs, $\tau_{long} \sim 1.9$ μs) has been attributed to weak coupling between D_0 and D_1.[41] Our interest here is not an accurate decomposition of the decay but rather an examination of the change in lifetime with increasing pump energy.

The bottom two decays depicted in Figure 6 of the benzyl radical–$(C_2H_4)_1$ species excited at higher energy show lifetimes shortened by an amount greater than the experimental uncertainty. The sharp feature appearing in the bottom decay is caused by an ionization laser generated one-color signal of aniline appearing in the cluster mass channel due to the laser delay scan and can
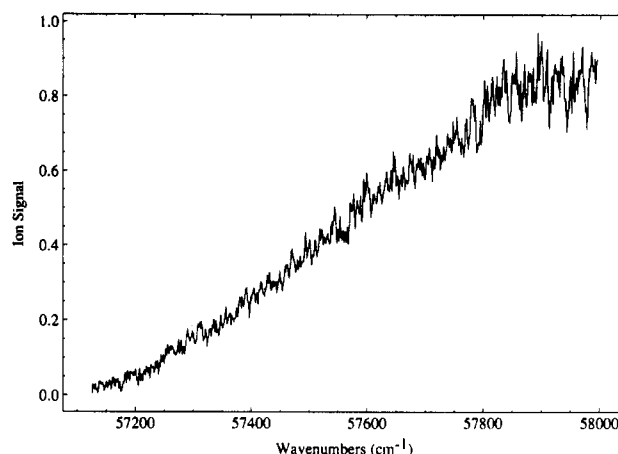
be ignored. The interpretation of the shortened benzyl radical–$(C_2H_4)_1$ lifetimes at increasing excitation energies in terms of cluster dissociation will be discussed below.

Another significant result which can be extracted from the benzyl radical–$(C_2H_4)_1$ decays of Figure 6 is that the observed long lifetimes rule out the possibility that homogeneous broadening processes cause the broad spectroscopic structure of Figures 4 and 5. The spectral broadening, therefore, can be assigned as due to a change in cluster structure and/or binding energy (i.e., a Franck–Condon shift in spectral intensity) upon optical excitation.

Figure 7 shows the ionization potential threshold spectra for benzyl radical–$(C_2H_4)_1$. The cluster threshold is shifted from the bare benzyl radical threshold by -1160 cm^{-1}.[27] This shift is significant more than the -50-cm^{-1} shift measured for the benzyl radical–$(C_2H_6)_1$ cluster. Furthermore, the broad nature of the ionization threshold ca. ~ 700 cm^{-1} differs significantly from that of the bare radical (~ 25 cm^{-1})[27] and the benzyl radical $(C_2H_6)_1$ cluster.[1] These differences in cluster ionization threshold are likely related to Franck–Condon effects and must be due to geometry differences within the excited neutral and ionic "cluster" species and serve as another property by which to distinguish the ethylene and ethane cluster behavior.

B. Proposed Model. In section IIIA, we present experimental data for benzyl radical–$(C_2H_4)_1$ which distinguish it from an "ordinary" van der Waals cluster; the benzyl radical–$(C_2H_4)_1$ species upon optical excitation exhibits a large excited-state "cluster binding energy" and a significant change in geometrical structure. These characteristics can be explained if it is postulated that a bimolecular addition reaction between the benzyl radical and ethylene occurs upon electronic excitation. This possibility is reasonable since for an exothermic bimolecular addition reaction it is necessary to have these conditions fulfilled—the data offer direct support for the suggested chemical reaction.

A model for this reaction can be readily generated. Figure 8 schematically represents the ground electronic-state interactions and reaction products for the benzyl radical–ethylene species. The energy scale of the reaction coordinate scheme is approximate, but Table 3 lists calculated relative energies for benzyl radical plus ethylene, 3-phenylpropyl radical, and α-ethylbenzyl radical (labeled in Figure 8 as I, IV, and VI, respectively). These energies are calculated using two different approaches: Benson's tables of bond enthalpies[32] and *ab initio* calculations. Agreement between the reaction energies using the two different approaches is good, quantitatively supporting the results obtained; forming 3-phenylpropyl radical or α-ethylbenzyl radical is energetically favored. The barriers to reaction generating these species, labeled III and V in Figure 8, are unknown, but since the generation of 3-phenylpropyl radical entails only bond formation, this path
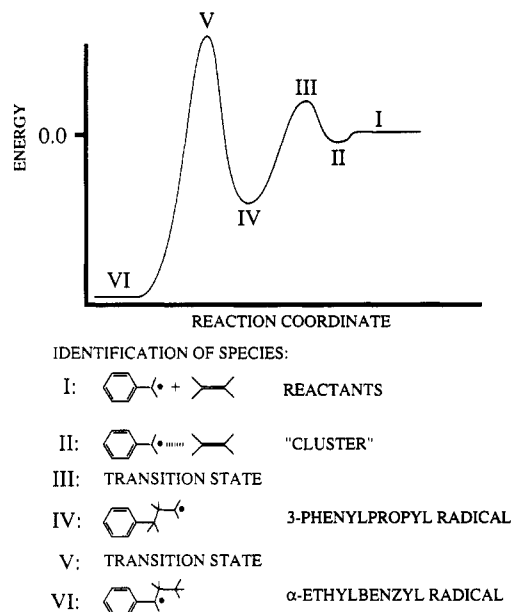
IDENTIFICATION OF SPECIES:

I: ⬡—(• +)=<   REACTANTS

II: ⬡—(•·····)=<   "CLUSTER"

III: TRANSITION STATE

IV: ⬡—ᴵᴵ•   3-PHENYLPROPYL RADICAL

V: TRANSITION STATE

VI: ⬡—ᴵᴵᴵ   α-ETHYLBENZYL RADICAL

Figure 8. Proposed reaction coordinate scheme for benzyl radical/ethylene. The reaction coordinate is arbitrary; however, the calculated relative energies of species **I**, **IV**, and **VI** are used to generate a realistic plot; see Table 3.

may possess an energetically low barrier to reaction. The subsequent formation of α-ethylbenzyl radical must proceed through either a highly contorted transition state or the formation of 3-phenylpropyl radical followed by a [1,3]-hydrogen shift. In either instance one can expect a large barrier to the formation of the thermodynamically favored product,[42] and thus we focus our attention here on the generation of 3-phenylpropyl radical. The benzyl-d_7 radical–$(C_2H_4)_1$ MRES data support the formation of 3-phenylpropyl radical and not α-ethylbenzyl radical; one would expect that H/D substitution would have a significant effect on the observed spectra and lifetimes if a hydrogen atom shift were part of the observed cluster behavior.

As pointed out above, the supersonic expansion is capable of cooling reaction products and clusters with ~70 kcal/mol of excess energy. One can thereby safely assume that the benzyl radical/ethylene clusters are cold and that if the 3-phenylpropyl ($\Delta H \sim -14$ kcal/mol) or the α-ethylbenzyl radical ($\Delta H \sim -20$ kcal/mol) were produced at the nozzle, it would be cooled in the expansion. Either of these cold radicals should generate sharp spectra and a well-defined ionization threshold.

Thus, the model we pursue calculationally to rationalize the observed data by the following set of assumptions: (1) no reaction occurs in the ground state between benzyl radical and ethylene because of the large assumed barrier (**III** of Figure 8) along the reaction coordinate, (2) the ground state cluster is cold, (3) the reaction observed is toward the 3-phenylpropyl radical (**IV** of Figure 8), and (4) the cluster is accessed in the excited state along the **II–III–IV** reaction coordinate as is appropriate from the Franck–Condon principle. The cluster is thus a van der Waals species in the ground state but a productlike 3-phenylpropyl radical species in the excited state.

C. Calculations. The electronic-state dependence of the addition reaction between benzyl radical and ethylene can be explored using *ab initio* computational techniques. The relevant results we wish to extract from calculations are the adiabatic reaction energies and barrier heights for the lowest three electronic states of the benzyl radical. This is an arduous task. Previous studies[1] have shown that an accurate description of these electronic states of the benzyl radical requires the contribution of many configuration-state functions (CSFs), making multiconfigurational techniques a necessity; furthermore, to quantify bond strengths accurately, which is necessary when examining chemical reactions, dynamic electron correlation effects must be considered. Therefore, the desired calculational technique to pursue is a multireference configuration interaction (MRCI) approach. Performing calculations at this level for benzyl radical/ethylene is prohibitively expensive (time and resources), and therefore approximations must be invoked. Our approach is to estimated dynamic electron correlation effects for reactant, transition state, and product species by taking the difference between ground-state PMP2[25] and PUHF results. These ground electronic-state dynamic electron correlation "correction energies" are then used with CASSCF excited-state results to infer more accurate reaction energies and barrier heights. The accuracy of this approximation must be examined. A logical start is to examine a simpler reaction system in order to calibrate (or test) the approach and results. We choose the methyl radical/ethylene system, for which the heat of reaction and barrier height along the reaction coordinate are known, as the test case for this approach.

In the later part of this subsection, the experimentally observed benzyl radical–$(C_2H_4)_1$ "apparent" binding energy and shortened lifetime data will be interpreted using the RRKM unimolecular dissociation rate approach.[33–38]

1. Methyl Radical plus Ethylene. Figure 9 depicts the addition of methyl radical to ethylene, with the one-dimensional reaction coordinate represented by r_1. Table 4 lists calculational results for this addition reaction in the ground electronic state using different levels of wave function approximation for a single basis set. The Dunning–Huzinaga double-zeta valence basis (DZV) has been used. The basis set superposition error (BSSE) is estimated using the couterpoise technique at the RHF/ROHF level. A BSSE of 4.3 kcal/mol for the propyl radical product species using a DZV basis is obtained. This value is somewhat large, but we consider it acceptable for the accuracy attempted here. The energies listed in Table 4 have not been corrected for BSSE. The columns of Table 4, from left to right, list energies for the separated methyl radical and ethylene fragments, the transition state, the propyl radical species, the derived adiabatic reaction energy, and the activation energy, respectively.

The first row of Table 4 contains a five-electron CASSCF result obtained by using the lone methyl radical orbital and electron, the ethylene (C–C) σ and π electrons and orbitals, and ethylene σ^* and π^* virtual orbitals. The subsequent three rows of Table 4 present augmentations and corrections to this basic approach. Comparing the calculated results to the experimentally derived vibrationally adiabatic reaction and activation energy of -25.5[43,44] and 6.4 kcal/mol,[45] respectively, an estimation of the calculation's success can be made.

From the five-electron CASSCF results listed in rows 1–4 of

TABLE 3: Calculation of Ground-State Reaction Enthalpies for Benzyl Radical plus Ethylene

species	reaction enthalpies[a]		*ab initio* calculations[b]	
	ΔH (kcal/mol)	relative ΔH (kcal/mol)	E (hartees)	relative E (kcal/mol)
reactants (I) (ethylene + benzyl)	57.5	0.0	−78.012 127 0 −269.044 801	0.0
reaction intermediate (IV) (3-phenylpropyl radical)	48.9	−8.6	−347.079 088	−13.8
product (VI) (α-ethylbenzyl)	34.0	−23.5	−347.091 655	−21.8

[a] Reference 32. [b] ROHF/RHF calculations using the Dunning–Huzinaga valence double-zeta (DZV) basis set. Figure 11 shows the calculated structures. The basis set superposition error for the 3-phenylpropyl radical species using the counterpoise technique is calculated to be 1.6 kcal/mol.

TABLE 4: *Ab Initio* Results for the Ground Electronic State Addition Reaction Methyl Radical + Ethylene → Propyl Radical[a]

	species energy (hartees)				
calculational technique	methyl radical + ethylene	transition state	propyl radical	ΔE(reaction)[b] (kcal/mol)	ΔE(activation)[b] (kcal/mol)
5-electron[c] CASSCF	−117.619 010	−117.592 672	−117.632 557	−8.5	16.5
MRCI/S+D (5e CASSCF structure)	−117.829 995	−117.815 192	−117.861 123	−19.5	9.3
MRCI/S+D[d] (optimized structure)	−117.831 559	−117.815 913	−117.862 757	−19.6	9.8
MRCI/S+D (Davidson correction)	−117.849 002	−117.836 947	−117.883 771	−21.8	7.6
3-electron[e] CASSCF	−117.592 371	−117.568 058	−117.612 110	−12.4	15.3
MRCI/S+D (3e CASSCF structure)	−117.828 891	−117.813 656	−117.857 979	−18.3	9.6
MRCI/S+D (Davidson correction)	−117.848 421	−117.837 217	−117.880 396	−20.1	7.0

[a] The 5-electron CASSCF results in 75 configuration state functions. Single and double excitations into the full virtual space (3 restricted core orbitals) results in 1 058 641 configurations. The 3-electron CASSCF results in 8 configuration state functions. Single and double excitations into the full virtual space (3 restricted core orbitals) results in 255 314 configurations. [b] Experimental values: ΔE(reaction) = −25.5 kcal/mol; ΔE(activation) = 6.4 kcal/mol (see text and refs 43, 44, and 45). [c] See Figure 9: ethylene + methyl radical, r_1 = 15.0 Å and r_2 = 1.3714 Å; transition state, r_1 = 2.2009 Å, r_2 = 1.4169 Å; propyl radical, r_1 = 1.5805 Å, r_2 = 1.5350 Å. [d] See Figure 9: ethylene + methyl radical, r_1 = 15.0 Å, r_2 = 1.3661 Å; transition state, r_1 = 2.2715 Å, r_2 = 1.4000 Å; propyl radical, r_1 = 1.5770 Å, r_2 = 1.5303 Å. [e] See Figure 9: ethylene + methyl radical, r_1 = 15.0 Å, r_2 = 1.3546 Å; transition state, r_1 = 2.2333 Å, r_2 = 1.3965 Å; propyl radical, r_1 = 1.5778 Å, r_2 = 1.5086 Å.

TABLE 5: *Ab Initio* Energies for the Excited Electronic State[a] Addition Reaction Methyl Radical + Ethylene → Propyl Radical; the DZV Basis Set and Five-Electron CASSCF Technique of Table 4 Are Employed[b] (See Figure 10 for Plot)

separation distance (Å)	5-electron CASSCF (hartees)	ΔE Relative (kcal/mol)	MRCI S+D (hartees)	ΔE relative (kcal/mol)	MRCI Davidson corr (hartees)	ΔE relative (kcal/mol)
15.0	−117.489 115	0.0	−117.689 030	0.0	−117.705 820	0.0
2.7	−117.502 562	−8.44	−117.718 953	−18.78	−117.739 265	−20.99
2.5	−117.508 222	−11.99	−117.728 980	−25.07	−117.749 576	−27.46
2.4	−117.511 424	−14.00	−117.734 265	−28.39	−117.756 225	−31.63
2.3714	−117.512 315	−14.56	−117.732 139	−27.05	−117.754 422	−30.50
2.2	−117.478 581	6.61	−117.687 335	1.06	−117.707 279	−0.92
2.1	−117.470 827	11.48	−117.681 186	4.92	−117.702 060	2.36
1.9	−117.434 993	33.96	−117.658 748	19.00	−117.681 367	15.35

[a] Excited electronic state of separated species is the $\pi\pi^*$ state of ethylene. [b] The 5-electron CASSCF results in 75 configuration state functions. Since and double excitations into the full virtual space (3 restricted core orbitals) result in 1 058 641 configurations. All internal degrees of freedom are optimized at the CASCF level for each separation distance.

Table 4 three important conclusions can be made. First, the effect of dynamic electron correlation on bond energy is significant since it decreases the activation energy by roughly a factor of 2 and the reaction energy by roughly a factor of $2^1/_2$. Second, the effect of dynamic electron correlation on the calculated structures is small. Third, the MRCI/S+D results agree quite well with the experimentally derived values, providing strong support for the calculational approach taken here. Similar results are obtained from the three-electron CASSCF/MRCI results presented in rows 5–7 of Table 4, for which the σ and σ^* orbitals of ethylene are not included. This calculational result is not unexpected since the ethylene σ orbitals do not participate significantly and the bond formation process.

The effect of electronic excitation on the addition reaction of methyl radical to ethylene is pursued to gain familiarity with this calculational approach for excited-state systems. The results are presented in Table 5 for fixed points along the reaction coordinate, r_1 (see Figure 9). For separated methyl radical and ethylene species, an electronic transition energy of 39 060 cm^{-1} can be extracted from Tables 4 and 5. This value compares favorably to the experimentally derived $^1A_g \leftarrow {}^1B_{1u}$ adiabatic transition energy of T_0 = 40 015 cm^{-1} for ethylene.[46] An inspection of the calculated results contained in the final column of Table 5 shows that no maxima are present along this reaction coordinate. This result contrasts with the ground electronic state result which identifies a single maximum. Furthermore, at r_1 = 2.3714 Å an apparent minimum is observed. Actually, an energy minimization of the entire complex (permitting r_1 to vary) experiences convergence problems for the CASSCF wave function. The difficulty is only partially alleviated by limiting the step size during geometry optimization to ~0.01 Å. We attributed this problem to "root flipping"; one can anticipate such calculational irregularities for an avoided crossing between electronic states. Indeed, the results of Table 5 support this conclusion: the excited state has no maximum and a single minimum along the reaction
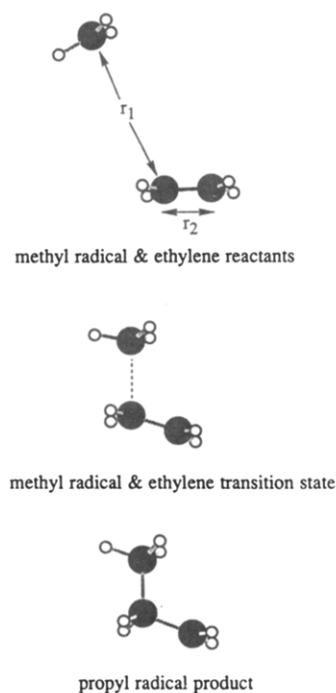

methyl radical & ethylene reactants

methyl radical & ethylene transition state

propyl radical product

Figure 9. Pictorial illustration of the reaction between methyl radical and ethylene. r_1 is the reaction coordinate in this simplified scheme.

coordinate and the ground state has a single maximum along the same coordinate at the same valve as the excited state minimum. A pictorial representation of the ground and excited electronic state reaction coordinate between methyl radical–ethylene is illustrated in Figure 10.

2. Benzyl Radical plus Ethylene. The methyl radical/ethylene results just discussed encourage our pursuit of benzyl radical/
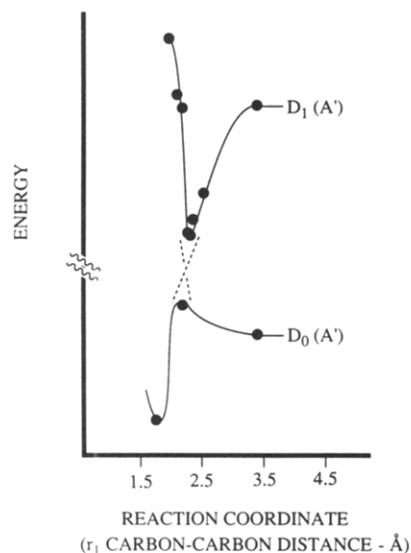
Figure 10. Calculated reaction coordinate between methyl radical and ethylene in the ground and first excited electronic states. (The ethylene species undergoes electronic excitation.) See Tables 4 and 5 and Figure 9.

ethylene calculations for the following reason: when the effects of dynamic electron correlation are taken into account, the CASSCF framework provides results for a reaction path which are in excellent agreement with experiment. We now estimate the magnitude of dynamic electron correlation for benzyl radical/ethylene.

Table 6 lists results of PMP2 calculations using spin annihilation up to $s + 6$ for the methyl radical/ethylene and benzyl radical/ethylene systems.[25] The PUHF methyl radical/ethylene results yield a reaction exothermicity close to that observed; however, a barrierless process leading to product formation is calculated which disagrees with experiment. At the PMP2 level, both the calculated reaction and activation energies are close to those observed. In some sense this agreement is fortuitous, since the PUHF results demonstrate the failure of the single determinental wave function approximation for this system, as static electron correlation alone is expected to overestimate the transition-state energy and underestimate the heat of reaction.[47] The same trend can be observed for the benzyl radical/ethylene system from a comparison between the results of Tables 3 and 6. The bottom of Table 6 lists the "corrected" benzyl radical/ethylene reaction and activation energies. These numbers are obtained by correcting PMP2 benzyl radical/ethylene results with the differences between methyl radical/ethylene PMP2 calculated and experimental reaction and activation energies. Finally, the RHF/ROHF determined BSSE for 3-phenylpropyl radical is 1.6 kcal/mol, smaller than for propyl radical, which is likely due to the longer α–β carbon–carbon bond length of ~0.05 Å used.

Figure 11 presents the reaction coordinate for the addition reaction between benzyl radical–ethylene. Table 7 lists CASSCF
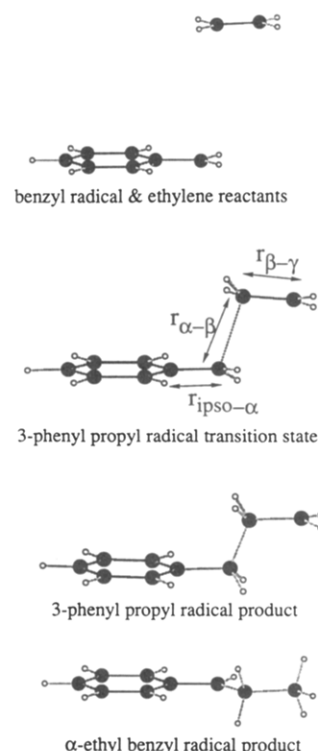

Figure 11. Pictorial illustration of the reaction between benzyl radical and ethylene. The reaction coordinate is $r_{\alpha-\beta}$.

calculational results for this reaction using the DZV basis set for the lowest three electronic states of the benzyl radical–ethylene system. The columns of Table 7 are analogous to those of Table 4. Table 7 also includes pertinent bond distances for the addition reaction. The results in Table 7 present several important points worth mentioning. The adiabatic reaction and activation energies for the three lowest electronic states are given in the last two columns of Table 7. The CASSCF results are listed, along with numbers (in parentheses) which are obtained by the addition of dynamic electronic correlation effects to the latter. Specifically, the correction is generated as follows: the ground electronic state reaction and activation energies are taken from Table 6, and the difference between these numbers and the ground electronic state CASSCF result yields the dynamic electron correlation contribution to the energy. This correction is used to estimate the excited electronic state reaction energetics. These "corrected" numbers are given in parenthesis in the last two columns. The 2A' state reaction is exothermic by 6.8 kcal/mol with a small barrier to reaction of 2.1 kcal/mol. The 1A'' state reaction, conversely, remains highly endothermic throughout. The possibility of an excited electronic state enhancement in reactivity exists for the 2A' state. Examining the barriers, the 1A' state has a significant barrier to reaction, whereas the 2A' state has a small barrier which may vanish upon accounting for zero-point energy effects.

TABLE 6: *Ab Initio* Perturbation Results for the Ground Electronic State Reaction Coordinate: Methyl Radical plus Ethylene and Benzyl Radical plus Ethylene

calculational technique	species energy (hartees)			ΔE(reaction) (kcal/mol)	ΔE(activation) (kcal/mol)
	radical + ethylene	transition state	product		
	Methyl Radical + Ethylene[a]				
PUHF	−117.566 166	−117.567 023	−117.601 441	−22.1	−0.54
PMP2	−117.806 387	−117.795 840	−117.839 084	−20.5	6.6
			expt:[a]	−25.5	6.4
			diff:[b]	5.0	0.2
	Benzyl Radical + Ethylene				
PUHF	−347.118 502	−347.103 064	−347.083 348	22.0	9.7
PMP2	−347.782 632	−347.764 285	−347.807 666	−15.7	11.5
			corr:[c]	−20.7	11.3

[a] See text and refs 43–45. [b] Obtained from PMP2 minus experimental results. [c] Obtained from the benzyl radical/ethylene PMP2 results and corrected by difference between the methyl radical/ethylene PMP2 calculated and experimental results.

TABLE 7: *Ab Initio* Potential Energy Surface Results for Benzyl Radical plus Ethylene Addition Reaction at the CASSCF Level[a]

calculational technique	species energy (hartees) and bond distances (Å)			ΔE(reaction)[b] (kcal/mol)	ΔE(activation)[b] (kcal/mol)
	benzyl radical + ethylene	transition state	3-phenylpropyl radical		
A′ electronic state; first root 9-electron CASSCF	−347.171683	−347.143098[c]	−347.171945	−0.2 (−20.7)	17.9 (11.3)
$r_{\alpha-\beta}$		2.3	1.5875		
$r_{ipso-\alpha}$	1.4199		1.5135		
$r_{\beta-\gamma}$	1.3547		1.5061		
A′ electronic state; second root 9-electron CASSCF	−347.067573	−347.053771	−347.045680	13.7 (−6.8)	8.7 (2.1)
$r_{\alpha-\beta}$		2.3144	1.6238		
$r_{ipso-\alpha}$	1.4508	1.4192	1.4946		
$r_{\beta-\gamma}$	1.3547	1.4821	1.4981		
A″ electronic state; first root 9-electron CASSCF	−347.064041		−347.000587	39.8 (19.3)	
$r_{\alpha-\beta}$			1.6002		
$r_{ipso-\alpha}$	1.3622		1.5053		
$r_{\beta-\gamma}$	1.3547		1.5038		

[a] Active space chosen: 28-core 4-doubly-occupied 1-radical 4-valence 37-frozen valence. The 9-electron CASSCF results in 4445 configuration state functions of A′ symmetry and 4312 configuration state functions of A″ symmetry. [b] The approximate numbers in parentheses represent the dynamic electronic correlation corrected result. The correction factors used are obtained from the methyl radical plus ethylene system (see Table 6). [c] This represents a lower-energy limit since the saddle point calculation did not converge.
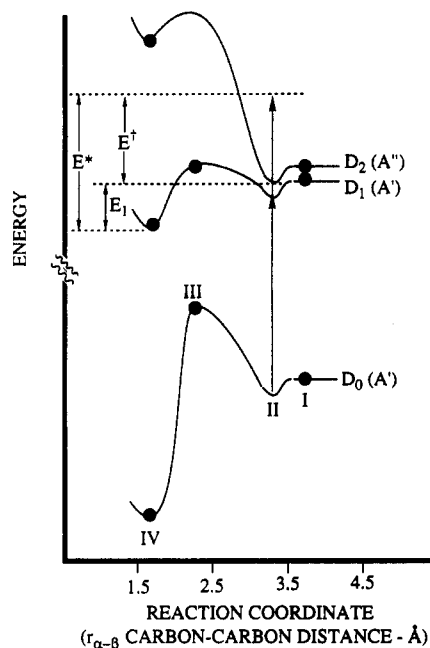

Figure 12. Calculated reaction coordinate between benzyl radical and ethylene in the ground and first two excited electronic states. (The benzyl radical species undergoes electronic excitation.) The values of ΔE used in this plot are the correlation energy corrected numbers of the last two columns of Table 7. The roman numerals depict ground state species that are identified in Figure 8.

Furthermore, the methyl radical/ethylene results contained in Tables 4 and 5 indicate that the contribution of dynamic electron correlation in an excited state is larger than in the ground electronic state, which also would decrease the barrier to reaction and estimated reaction exothermicity even further. This result is important, since it yields insight into what could cause the experimentally observed phenomena of high binding energy and dramatic change in equilibrium structure. Figure 12 illustrates the calculated adiabatic reaction coordinate energetics for the addition of benzyl radical to ethylene. We suggest that upon optical excitation of the cold cluster, a simultaneous change in cluster equilibrium structure, and an enhancement in cluster binding energy (bond formation) occur. Any vibronic interaction between the two close-lying excited states would further enhance reactivity and structural changes.

3. Dissociation Kinetics of Electronically Excited Benzyl Radical/(Ethylene)$_1$. The calculational results presented in the last section support the proposed physical model in which optical excitation of a cold benzyl radical/ethylene cluster leads to an excited-state chemical reaction. Because energy is conserved

within the cluster in the experiments performed here, a cold 3-phenylpropyl radical product is not formed. A remaining issue to be examined is an interpretation of the loss of signal in the cluster mass channel at energies above 36 200 cm⁻¹ and an apparently associated decrease in cluster excited-state lifetime above 32 780 cm⁻¹. At these energies the cluster would have roughly 30 and 40 kcal/mol of vibrational energy in the excited electronic state, assuming that the origin of the transition is at 21 800 cm⁻¹.

If one assumes the cluster or incipient excited state molecule can dissociate with an RRKM mechanism, then one can convert the reduced lifetimes to a value for the binding or bond energy. Within this approximation, the energy values defined in Figure 12 are the cluster binding energy (E_1), the vibrational energy in the cluster (E^*), and the difference between these $(E^* - E_1 = E^\dagger)$, the excess energy in the cluster.[48] Table 7 lists the calculated dissociation rates based on MOPAC 6.0[49] calculated vibrational energies for the 3-phenylpropyl radical product and a direct count algorithm for the density of states at E^*, $N(E^*)$, and sum of states at $E^\dagger$, $\sum P(E^\dagger)$.[33,38]

The relevant experimental lifetimes to compare to the calculational results are obtained by noting that, at an excitation energy of 22 300 cm⁻¹, $\tau = 1.1~\mu s$ and no dissociation can occur. This time, therefore, represents the intrinsic excited-state lifetime without dissociation of the complex. At the higher excitation energies the measured lifetimes arises from both dissociation and fluorescence; hence $k_{meas} = k_{fluor} + k_{dissoc}$. Using $k = 1/\tau$ and the lifetimes given in Figure 6, the observed rate constants presented in Table 8 are obtained. The value of <1 ns for the 39.1 kcal/mol excitation energy represents the temporal resolution of our laser system. The RRKM expression is also evaluated using E_1 fixed at the *ab initio* estimated value of 6.8 kcal/mol, which results in calculated rates roughly 3 orders of magnitude faster than those observed.

Three important results can be extracted from the results of Table 8. First, a large variation in lifetime as a function of binding energy E_1 is observed. Second, a fitted value of E_1 of 19.0 kcal/mol is intuitively reasonable and falls within the energy region expected, assuming that we have underestimated dynamic electron correlation effects. Third, this mechanism cannot explain all the observed lifetimes. This latter point implies that an additional depletion mechanism at high energy (such as another electronic state, internal conversion, etc.) may exist for the complex. Indeed, a 2^2A_2 benzyl radical electronic state is present at $E^\dagger \sim 32$ kcal/mol, consistent with our experimental observations.

IV. Conclusions

The benzyl radical/ethylene molecular cluster is generated using nozzle photolysis/supersonic jet cooling techniques and is

TABLE 8: Calculation of Excited State Binding Energy from Observed Benzyl Radical/Ethylene Vibrational Predissociation Lifetimes Based on an RRKM Treatment[a] (See Ref 48)

$E^\dagger$ (kcal/mol)	E^* (kcal/mol)	$\Sigma P(E^\dagger)$	$N(E^*)$	rate constant (s^{-1}) calc	rate constant (s^{-1}) obsd
−2.0	17.0		2.6×10^{10}		9.1×10^5
29.4	48.4	1.7×10^{14}	5.0×10^{18}	1.0×10^6	1.2×10^6
31.7	50.7	7.2×10^{14}	1.5×10^{19}	1.4×10^6	1.4×10^6
39.1	58.1	4.6×10^{16}	3.8×10^{20}	3.6×10^6	$>1 \times 10^9$

[a] Dissociation rate obtained using $k = (1/h)(\Sigma P(E^\dagger)/N(E^*))$. State densities given per wavenumber. $E_1 = 19.0$ kcal/mol (fitted value).

probed using MRES, ionization potential threshold, and laser delay measurements. The experimental cluster data consist of spectrally broad MRES, an excited state which remains intact with an excess of vibrational energy of 11 810 cm^{-1}, a red-shifted ionization threshold of −1160 cm^{-1}, and excited-state lifetimes of ∼1 μs. This collection of data is not consistent with a van der Waals type bonding in both the ground and excited electronic states. We instead interpret the excited-state behavior as due to a bimolecular addition reaction occurring upon optical excitation of the cold, van der Waals-like, ground-state cluster.

Ab initio calculations for the methyl radical/ethylene and benzyl radical/ethylene systems have lent insight into the excited electronic state chemical reactivity. Quantitatively accurate results have been obtained for methyl radical plus ethylene at the CASSCF/MRCI level. The inclusion of dynamic electron correlation effects is necessary to determine bond strengths accurately but has little effect on the optimized structures. For benzyl radical/ethylene, dynamic electron correlation effects have been estimated by PMP2 calculations and, when combined with CASSCF results, generate an excited-state system with a small barrier to reaction and a reaction exothermicity of 6.8 kcal/mol in the 2A′ excited state. These results are qualitatively consistent with the experimental observations. Note that the dynamic electron correlation corrections applied to the excited state are most likely too small, and more accurate corrections should further lower the activation barrier and increase the reaction exothermicity.

Excited electronic state lifetime measurements as a function of excess vibrational energy in D$_1$ have been used to extract an excited-state cluster binding energy using RRKM theory. Conceptually, in the absence of collisions which may dissipate the heat of reaction, the observed lifetime of the complex is determined solely by the density of states at the excitation energy and the sum of states at dissociation.

References and Notes

(1) Disselkamp, R.; Bernstein, E. R. *J. Chem. Phys.* **1993**, *98*, 4339.
(2) Turro, N. J. *Modern Molecular Photochemistry*; Benjamin/Cummings: Menlo Park, CA, 1978.
(3) Salem, L. *Electrons in Chemical Reactions, First Principles*; John Wiley & Sons: New York, 1982.
(4) Brooks, P. R. *J. Chem. Phys.* **1969**, *50*, 5031.
(5) Brooks, P. R. *Science* **1976**, *193*, 11.
(6) Buehler, R. J.; Bernstein, R. B. *J. Chem. Phys.* **1969**, *51*, 5305.

(7) Rulis, A. M.; Wilcomb, B. E.; Bernstein, R. B. *J. Chem. Phys.* **1974**, *60*, 2822.
(8) Van den Ende, D.; Stolte, S. *Chem. Phys. Lett.* **1980**, *76*, 13.
(9) Karny, Z.; Estler, R. C.; Zare, R. N. *J. Chem. Phys.* **1978**, *69*, 5199.
(10) Rettner, C. T.; Zare, R. N. *J. Chem. Phys.* **1982**, *77*, 2416.
(11) Radhakrishnan, G.; Buelow, S.; Wittig, C. *J. Chem. Phys.* **1986**, *84*, 727.
(12) Bernardi, F.; Bottoni, A.; Field, M. J.; Guest, M. F.; Hillier, I. H.; Robb, M. A.; Venturini, A. *J. Am. Chem. Soc.* **1988**, *110*, 3050.
(13) (a) McDouall, J. J. W.; Robb, M. A.; Niazi, U.; Bernardi, F.; Schlegel, H. B. *J. Am. Chem. Soc.* **1987**, *109*, 4642. (b) Ionov, S. I.; Brucker, G. A.; Jaques, C.; Vala-Chovic, L.; Wittig, C. *J. Chem. Phys.* **1992**, *97*, 9486. (c) Bohmer, E.; Shin, S. K.; Chen, Y.; Wittig, C. *J. Chem. Phys.* **1992**, *97*, 2536. (d) Wittig, C.; Sharpe, S.; Beaudet, R. A. *Acc. Chem. Res.* **1988**, *21*, 341.
(14) Houk, K. N.; Lin, Y. T.; Brown, F. K. *J. Am. Chem. Soc.* **1986**, *108*, 554.
(15) Komornicki, A.; Goddard, J. D.; Schaefer, H. F. *J. Am. Chem. Soc.* **1980**, *102*, 1763.
(16) Bernardi, F.; Olivucci, M.; McDouall, J. J. W.; Robb, M. A. *J. Am. Chem. Soc.* **1987**, *109*, 544.
(17) Bernardi, F.; Bottoni, A.; Olivucci, M.; Robb, M. A.; Schlegel, H. B.; Tonachini, G. *J. Am. Chem. Soc.* **1988**, *110*, 5993.
(18) Boutalib, A.; Gadea, F. X. *J. Chem. Phys.* **1992**, *97*, 1144.
(19) Lowdin, P. O. *Phys. Rev.* **1955**, *97*, 1509.
(20) Arnaud, R.; Barone, V.; Olivella, S.; Sole, A. *Chem. Phys. Lett.* **1985**, *118*, 573.
(21) Gonzalez, C.; Sosa, C.; Schlegel, H. B. *J. Phys. Chem.* **1989**, *93*, 2435.
(22) Shang, Q.-Y.; Moreno, P. O.; Bernstein, E. R. *J. Am. Chem. Soc.*, in press.
(23) Dupuis, M.; Marquez, A. HONDO 8.4 (IBM Corporation, Department MLM/428, Neighborhood Road, Kingston, NY 12401), 1992.
(24) Saxe, P.; Martin, R. (Los Alamos National Laboratory, Los Alamos, NM), Page, M. (Naval Research Laboratory, Washington, DC), Lengsfield, B. H., III (Lawrence Livermore National Laboratory, Livermore, CA), MESA 3.1, 1993.
(25) Gaussian 92, Revision C.4: Frisch, M. J.; Trucks, G. W.; Head-Gordon, M.; Gill, P. M. W.; Wong, M. W.; Foresman, J. B.; Johnson, B. G.; Schlegel, H. B.; Robb, M. A.; Replogle, E. S.; Gomperts, R.; Andres, J. L.; Raghavachari, K.; Binkley, J. S.; Stewart, J. J. P.; Pople, J. A. Gaussian Inc., Pittsburgh, PA, 1992.
(26) *Methods of Electronic Structure Theory*; Schaefer, H. F., Ed.; Plenum Press: New York, 1977; Chapter 1 and Appendix 2.
(27) Im, H.-S.; Bernstein, E. R. *J. Chem. Phys.* **1991**, *95*, 6326.
(28) Cossart-Magos, C.; Leach, S. *J. Chem. Phys.* **1976**, *64*, 4006.
(29) Negri, F.; Orlandi, G.; Zerbetto, F.; Zgierski, M. Z. *J. Chem. Phys.* **1990**, *93*, 600.
(30) Seeman, J. I.; Grassian, V. H.; Bernstein, E. R. *J. Am. Chem. Soc.* **1988**, *110*, 8542.
(31) Grassian, V. H.; Bernstein, E. R.; Secor, H. V.; Seeman, J. I. *J. Phys. Chem.* **1989**, *93*, 3470.
(32) Benson, S. W. *Thermochemical Kinetics, Methods for the Estimation of Thermochemical Data and Rate Parameters*, 2nd ed.; John Wiley & Sons: New York, 1976.
(33) Hineman, M. F.; Bernstein, E. R.; Kelley, D. F. *J. Chem. Phys.* **1993**, *98*, 2516.
(34) Felker, P. M.; Zewail, A. H. *Adv. Chem. Phys.* **1988**, *70*, 265 and references therein.
(35) Knee, J. L.; Kdlhundkar, L. R.; Zewail, A. H. *J. Chem. Phys.* **1987**, *87*, 115.
(36) Outhouse, E. A.; Bickel, G. A.; Dremmer, D. R.; Wallace, S. C. *J. Chem. Phys.* **1991**, *95*, 6261.
(37) Osborn, D. L.; Alfano, J. C.; van Dantzig, N.; Levy, D. H. *J. Chem. Phys.* **1992**, *97*, 2276.
(38) Nimlos, M. R.; Young, M. A.; Bernstein, E. R.; Kelley, D. F. *J. Chem. Phys.* **1988**, *91*, 5268.
(39) For discussion of calculation technique and van der Waals parameters, see ref 1. The partial charges on carbon and hydrogen atoms were taken to be −0.352 and 0.176 electron units, respectively.
(40) Fukushima, M.; Obi, K. *J. Chem. Phys.* **1990**, *93*, 8488.
(41) Lahmani, F.; Tramer, A.; Tric, C. *J. Chem. Phys.* **1974**, *60*, 4419, 4431.
(42) Bernardi, F.; Robb, M. A.; Schlegel, H. B.; Tonachini, G. *J. Am. Chem. Soc.* **1984**, *106*, 1198 and references therein.
(43) *J. Phys. Chem. Ref. Data, Suppl.* **1985**, *14*.
(44) Castelhano, A. L.; Griller, D. *J. Am. Chem. Soc.* **1982**, *104*, 3655.
(45) Kerr, J. A. *Free Radicals*; Kochi, J., Ed.; John Wiley & Sons: New York, 1972; Vol. 1.
(46) Herzberg, G. *Electronic Spectra of Polyatomic Molecules*; Van Norstrand Reinhold: New York, 1966.
(47) Rappe, A. K. Colorado State University, private communication.
(48) Robinson, P. J.; Holbrook, K. A. *Unimolecular Reactions*; Wiley-Interscience: New York, 1971.
(49) MOPAC 6.0, J. J. P. Stewart, Frank J. Seiler Research Laboratory, USAF, Colorado Springs, CO, 1990.